The Journal of Immunology

Association of CD147 and Calcium Exporter PMCA4 Uncouples IL-2 Expression from Early TCR Signaling

Verena Supper, Herbert B. Schiller, Wolfgang Paster, Florian Forster, Cyril Boulègue, Goran Mitulovic, Vladimir Leksa, Anna Ohradanova-Repic, Christian Machacek, Philipp Schatzlmaier, Gerhard J. Zlabinger and Hannes Stockinger

J Immunol 2016; 196:1387-1399; Prepublished online 4 January 2016;
doi: 10.4049/jimmunol.1501889
http://www.jimmunol.org/content/196/3/1387

The Journal of Immunology is published twice each month by
The American Association of Immunologists, Inc.,
1451 Rockville Pike, Suite 650, Rockville, MD 20852

Print ISSN: 0022-1767 Online ISSN: 1550-6606.

Association of CD147 and Calcium Exporter PMCA4 Uncouples IL-2 Expression from Early TCR Signaling

Verena Supper,* Herbert B. Schiller,*,[1] Wolfgang Paster,* Florian Forster,* Cyril Boulègue,[†] Goran Mitulovic,[‡] Vladimir Leksa,*,[§] Anna Ohradanova-Repic,* Christian Machacek,* Philipp Schatzlmaier,* Gerhard J. Zlabinger,[¶] and Hannes Stockinger*

The Ig superfamily member CD147 is upregulated following T cell activation and was shown to serve as a negative regulator of T cell proliferation. Thus, Abs targeting CD147 are being tested as new treatment strategies for cancer and autoimmune diseases. How CD147 mediates immunosuppression and whether association with other coreceptor complexes is needed have remained unknown. In the current study, we show that silencing of CD147 in human T cells increases IL-2 production without affecting the TCR proximal signaling components. We mapped the immunosuppressive moieties of CD147 to its transmembrane domain and Ig-like domain II. Using affinity purification combined with mass spectrometry, we determined the domain specificity of CD147 interaction partners and identified the calcium exporter plasma membrane calcium ATPase isoform 4 (PMCA4) as the interaction partner of the immunosuppressive moieties of CD147. CD147 does not control the proper membrane localization of PMCA4, but PMCA4 is essential for the CD147-dependent inhibition of IL-2 expression via a calcium-independent mechanism. In summary, our data show that CD147 interacts via its immunomodulatory domains with PMCA4 to bypass TCR proximal signaling and inhibit IL-2 expression. ***The Journal of Immunology*****, 2016, 196: 1387–1399.**

In the course of an adaptive immune response, a delicate combination of signaling components, signaling kinetics, and strength determines T cell activation, proliferation, differentiation, or inactivation. A crucial hallmark of T cell activation is the induction of phospholipase Cγ (PLCγ) (1). PLCγ generates the second messengers diacylglycerol and inositol-1,4,5-triphosphate (IP3), which branches proximal signaling into three major downstream signaling routes, leading to production of the T cell growth factor IL-2. Diacylglycerol binding to protein kinase C (PKC) stimulates the ERK MAPK pathway and the NF-κB pathway, resulting in activation of the transcription factors Fos and NF-κB, respectively. At the same time, IP3 binding to IP3-mediated calcium channels at the endoplasmic reticulum (ER) leads to release of calcium from the ER and opening of store-operated calcium channels at the plasma membrane (2). A rise in cytosolic calcium levels enables complex formation of calcium-binding protein calmodulin with serine-threonine phosphatase calcineurin that dephosphorylates NFAT (reviewed in Ref. 3). At the same time, calmodulin stimulates calmodulin-dependent kinases to activate the NF-κB pathway through phosphorylation of NF-κB (4–6). The change in phosphorylation status of NFAT and NF-κB causes their nuclear translocation and, hence, their activity as transcription factor for their target genes, which include the T cell growth factor IL-2.

Several positive and negative regulatory mechanisms fine-tune TCR signaling. These involve the ligation of immunomodulatory coreceptors, such as CD28 and CTLA4 (reviewed in Ref. 7). CD28 stimulation, for example, enforces TCR signaling cascades by inducing the kinases PKC and PI3K or the G proteins via RasGRP. In contrast, the inhibitory receptor CTLA4 competes with CD28 for its ligand B7 and also activates the phosphatases PP2A and SHP2. These phosphatases dephosphorylate TCR proximal signaling components and, thereby, blunt TCR signaling at an early stage.

Similar to the inhibitory coreceptor CTLA4 (8), the Ig-like glycoprotein CD147 (also known as basigin, M6, EMMPRIN,

*Molecular Immunology Unit, Institute for Hygiene and Applied Immunology, Centre for Pathophysiology, Infectiology, and Immunology, Medical University of Vienna, 1090 Vienna, Austria; [†]Microchemistry Core Facility, Max Planck Institute of Biochemistry, 82152 Martinsried, Germany; [‡]Proteomics Core Facility, Medical University of Vienna, 1090 Vienna, Austria; [§]Institute of Molecular Biology, Slovak Academy of Sciences, 84551 Bratislava, Slovak Republic; and [¶]Institute of Immunology, Centre for Pathophysiology, Infectiology, and Immunology, Medical University of Vienna, 1090 Vienna, Austria

[1]Current address: Department of Proteomics and Signal Transduction, Max Planck Institute of Biochemistry, 82152 Martinsried, Germany.

ORCIDs: 0000-0003-1964-3965 (G.M.); 0000-0001-6404-4430 (H.S.).

Received for publication August 24, 2015. Accepted for publication November 25, 2015.

This work was supported by the GEN-AU-Program of the Austrian Federal Ministry of Science and Research (FA644A0103) and the Austrian Research Promotion Agency (Mobility Stipendium 831947). V.L. was supported by the Austrian Science Fund (P22908) and the Slovak Grant Agency (2/0063/14).

H.S. initiated the project; V.S., H.B.S., W.P., F.F., and H.S. designed the experiments; V.S., H.B.S., V.L., A.O.-R., and H.S. wrote the manuscript; V.S., F.F., C.B., G.M., C.M., and P.S. performed experiments; V.S., H.B.S., F.F., C.B., and G.M. analyzed data; W.P., F.F., H.B.S., C.B., G.M., and G.J.Z. provided important reagents and/or analytical tools; and all authors read and approved the manuscript.

The mass spectrometry proteomics data have been submitted to the ProteomeXchange Consortium ((http://www.ebi.ac.uk/pride/archive/) under accession numbers PXD003029 and 10.6019/PXD003029.

Address correspondence and reprint requests to Dr. Hannes Stockinger, Molecular Immunology Unit, Institute for Hygiene and Applied Immunology, Medical University of Vienna, Kinderspitalgasse 15, 1090 Vienna, Austria. E-mail address: hannes.stockinger@meduniwien.ac.at

The online version of this article contains supplemental material.

Abbreviations used in this article: AcN, acetonitrile; AP-MS, affinity purification–mass spectrometry; ER, endoplasmic reticulum; FA, formic acid; FDR, false discovery rate; HA, hemagglutinin; IP3, inositol-1,4,5-triphosphate; MS, mass spectrometry; PKC, protein kinase C; PLCγ, phospholipase Cγ; PMCA4, plasma membrane calcium ATPase isoform 4; qPCR, quantitative real-time PCR; RNAi, RNA interference; SEE, staphylococcal enterotoxin E; shControl, shRNA control; shRNA, short hairpin RNA.

TCSF, OK, or 5F7) is upregulated on activated T blasts (9–11). Furthermore, CD147 was shown to influence T cell proliferation (10–12), thymocyte maturation (13), NFAT transcriptional activity, and IL-2 production (14, 15). Recently, CD147 levels were described as a surrogate marker of activated regulatory T cells (16, 17), and Abs specific to the extracellular domain of CD147 showed potent immunomodulatory capacities (11, 18).

Although interaction partners of CD147 and associated mechanisms have been partially described, how CD147 is involved particularly in TCR signaling is not understood. Therefore, this study was designed to determine the immunomodulatory role and partners of CD147 in T cells that mediate CD147-dependent immune suppression. We now report that CD147 regulates T cell activation by forming a complex with the plasma membrane calcium ATPase isoform 4 (PMCA4) that decouples early TCR signaling from IL-2 expression.

Materials and Methods

Abs

The following mAbs were kindly provided by Vaclav Horejsi (Institute of Molecular Genetics, Academy of Sciences of the Czech Republic, Prague, Czech Republic): AFP-01 to α-fetoprotein, MEM-87 to CD8, MEM-18 to CD14, MEM-154 to CD16, WIN-19 to CD19, MEM-97 to CD20, MEM-101A to CD29, MEM-28 to CD45, MEM-188 to CD56, and MEM-M6/1 and MEM-M6/6 to CD147. The mAb to PMCA4 (Ja-9) was from Abcam (Cambridge, MA); the mAb to the hemagglutinin (HA) tag (05-904) was ordered from Millipore (Billerica, MA); the CD16 mAb VIFcRIII was purchased from Hölzel Diagnostika (Köln, Germany); and the CD3 mAb OKT3 was from Ortho Pharmaceuticals (Raritan, NJ). Clone Leu-28 to CD28 and the allophycocyanin-conjugated rat mAb against IL-2 (MQ1-17H12) were purchased from BD Biosciences (Franklin Lakes, NJ). The polyclonal Abs specific for PLCγ-1 and phospho–Y783-PLCγ-1 and the mAbs specific for phospho–Y416-Src (D49G4) and GAPDH (14C10) were purchased from Cell Signaling (Danvers, MA). The mAb to Lck (3A5) was purchased from Santa Cruz Biotechnology (Santa Cruz, CA). The polyclonal Ab to actin was purchased from Sigma-Aldrich (St. Louis, MO), and Beriglobin P was from Aventis Behring (King of Prussia, PA). Allophycocyanin-conjugated AffiniPure $F(ab')_2$ fragment goat anti-mouse IgG + IgM (H+L) was purchased from Jackson ImmunoResearch (West Grove, PA), goat anti-rabbit-HRP was from Bio-Rad (Hercules, CA), and goat anti-mouse–HRP was from Sigma-Aldrich. Biotin conjugation of Abs was achieved with EZ-Link Sulfo-NHS-SS-Biotin (Thermo Scientific, Rockford, IL), in accordance with the manufacturer's protocol.

Reagents

PMA, ionomycin calcium salt (ionomycin) from *Streptomyces conglobatus*, and thapsigargin were purchased from Sigma-Aldrich. Staphylococcal enterotoxin E (SEE) was purchased from Toxin Technology (Sarasota, FL), and the protease inhibitor mixture was from Roche (Basel, Switzerland).

Cell culture

The human leukemic T cell line Jurkat E6.1, the human leukemic B cell line Raji, and the human embryonic kidney cell line HEK 293T were obtained from the American Type Culture Collection (Manassas, VA). The Jurkat T cell clone IL-2–Luc stably transfected with an IL-2 promoter luciferase reporter construct was the kind gift of Thomas Baumruker (Novartis Institutes for BioMedical Research, Vienna, Austria). The Jurkat T cell clone NFAT-Luc stably transfected with an IL-2 minimal promoter luciferase reporter construct with three tandem copies of the NFAT1-binding site was the kind gift of Michel J. Tremblay (Centre Hospitalier de l'Université Laval Research Center, Laval University, Quebec, Canada). The Jurkat T cell clones NFAT-EGFP and NF-κB–Luc were generated in our laboratory by transfection of pNFAT-EGFP (a kind gift from Johannes Schmid, Center for Physiology and Pharmacology, Medical University of Vienna, Austria) or the pNFκB-Luc pathfinder construct from Stratagene (Agilent Technologies, Santa Clara, CA). Cell lines were cultured as previously described (19).

Human PBMCs were isolated from the blood of healthy donors by standard density-gradient centrifugation using Lymphoprep (Nycomed, Oslo, Norway). To stimulate growth of human peripheral blood T cells, the freshly isolated mononuclear cells were stimulated with plate-bound CD3 mAb OKT3 (1 μg/ml) and soluble CD28 mAb Leu-28 (0.5 μg/ml) for 5 d. For coimmunoprecipitation experiments, $CD4^+$ T cells were isolated using the magnetic cell sorting system Vario MACS (Miltenyi Biotec, Bergisch Gladbach, Germany) by negative depletion for cytotoxic T cells, phagocytic cells, B cells, and NK cells, as described earlier (20). Primary cells were maintained in RPMI 1640 medium supplemented with 5% heat-inactivated FCS (Invitrogen), 100 U/ml penicillin, 100 μg/ml streptomycin, and 2 mM L-glutamine.

Plasmids

The lentiviral short hairpin RNA (shRNA) expression vector pLKO.1 puro was kindly provided by Sheila Stewart (Washington University School of Medicine, St. Louis, MO). To generate pLKO-puro-shCD147 containing an shRNA construct specific for human CD147, shCD147sense (5′-CCGGTGTCGTCAGAACACATCAACTTCAAGAGAGTTGATGTGTTCTGACGACTTTTTG-3′) and shCD147 antisense (5′-CAAAAAGTCGTCAGAACACATCAACTCTCTTGAAGTTGATGTGTTCTGACGACACCGG-3′) were annealed and cloned via EcoRI/AgeI into pLKO.1 puro. The nontarget shRNA construct pLKO-puro_ntCtr (shRNA control [shControl]) was from the German Science Center for Genome Research. The plasma membrane calcium exporters and cofilin were silenced using retroviral pSM2 vectors from the human shRNA library 1.3-1.15 (21) (Open Biosystems, Huntsville, AL) containing the following shRNA sequence: PMCA4_P1 5′-TGCTGTTGACAGTGAGCGCCCGGACTATCTGCATAGCTTATAGTGAAGCCACAGATGTATAAGCTATGCAGATAGTCCGGATGCCTACTGCCTCGGA-3′,PMCA4_P2 5′-TGCTGTTGACAGTGAGCGCGGTGATATTGCCCAAGTCAAATAGTGAAGCCACAGATGTATTTGACTTGGGCAATATCACCATGCCTACTGCCTCGGA-3′, PMCA1_P1 5′-TGCTGTTGACAGTGAGCGCCCTCGTCACGTTGGTAATAAATAGTGAAGCCACAGATGTATTTATTACCAACGTGACGAGGTTGCCTACTGCCTCGGA-3′, and Cofilin 5′-TGCTGTTGACAGTGAGCGACCTGAGTGAGGACAAGAAGAATAGTGAAGCCACAGATGTATTCTTCTTGTCCTCACTCAGGCTGCCTACTGCCTCGGA-3′.

The lentiviral and retroviral helper plasmids are detailed in (19). All deletion and swap mutants of CD147 were prepared in the retroviral expression vector pBMN-IRES-GFP (kindly provided by Gary Nolan, Stanford University School of Medicine, Stanford, CA). Full-length CD147 was mutated using the QuikChange Site-Directed Mutagenesis Kit (Agilent Technologies) and the forward primer (5′-GGCCGTGAAGTCGTCTGAGCATATCAACGAGGGGGAG-3′) and reverse primer (5′-CTCCCCCTCGTTGATATGCTCAGACGACTTCACGGCC-3′) bearing the silent point mutations. From this construct we generated the mutants illustrated in Fig. 3A. HA-tagged CD147 mutants were generated by insertion of the TAP tag from the pfMSCV Strep3xHA plasmid at the 3′ end of the signal sequence of CD147 by gene synthesis. All primers and sequences are available upon request.

Gene transfer to Jurkat and primary T cells

Gene delivery was achieved using viral transduction, as previously described by Muhammad et al. (22).

Quantitative PCR

For quantitative real-time PCR (qPCR) analysis, RNA was isolated using TRIzol reagent (Invitrogen) and transcribed with the SuperScript III Reverse Transcriptase System (Invitrogen, Life Technologies), and qPCR was performed using GoTaq qPCR Master Mix (Promega, Fitchburg, WI) on a CFX96 Real-Time PCR System (Bio-Rad). The following primer sets were used for qPCR reactions: CD147 (forward: 5′-GACGACCAGTGGGGAGAGTA-3′, reverse: 5′-CGTTGATGTGTTCTGACGACTTC-3′), PMCA4 (forward: 5′-CAGTAGACTGAAAACCTCCCCT-3′, reverse: 5′-GATGATAAGCGTGACATCTTGA-3′), PMCA1 (forward: 5′-AGATGGAGCTATTGAGAATCGCA-3′, reverse: 5′-GCCAGTTTTGTAAGTTTCCCTTG-3′), and GAPDH (forward: 5′-AAGGTGAAGGTCGGAGTCAAC-3′, reverse: 5′-GGGGTCATTGATGGCAACAATA-3′).

Flow cytometry

Immunofluorescence analysis of cells was done according to the protocol described by Muhammad et al. (22). The cells were analyzed on an LSR II flow cytometer (BD Biosciences, Franklin Lakes, NJ), and the data were processed using FlowJo software (TreeStar, Ashland, OR).

Intracellular IL-2 measurement

Jurkat T cells were stimulated for 6 h, and secretion of IL-2 was blocked for the last 4 h with 0.3 μM monensin (Sigma-Aldrich). Cells were fixed with 4% paraformaldehyde and stained on ice with 5 μg/ml anti–IL-2 mAb in PBS, 5% FCS, and 0.1% saponin. Intracellular IL-2 staining was analyzed using flow cytometry, as described above.

Calcium flux measurement

Jurkat T cells were stained with 1 μM calcium-sensitive and cell permeable Indo-1, AM (Molecular Probes/Life Technologies). The cells were analyzed as previously described (23) on an LSR II flow cytometer (BD Biosciences). In brief, the calcium-sensitive dye Indo-1 was excited with a UV laser, Ca^{2+}-free Indo-1 signals were detected with a 530/30 filter, and Ca^{2+}-bound Indo-1 emission was detected with a 405/20 filter. The emission values were used to calculate the ratio 405/530. Five minutes before the measurement, cells were warmed to 37°C in a water bath, and calcium fluxes were assessed at 37°C in a tube jacket (100–1000 cells/time point). In total, several tens of thousands of cells (depending on the experiment and measurement length) were measured for one graph. The baseline was measured for 15–30 s before the reagents were added. Data were processed using FlowJo software (TreeStar). For some experiments, Jurkat T cells were labeled first with 20 nM CFSE; after washing, $CFSE^{-}$ and CFSE-labeled cells were pooled before they were stained with 1 μM cell permeable Indo-1, AM.

Quantification of nuclear NFAT levels

Jurkat T cells expressing an NFAT-EGFP fusion protein were stimulated with PMA (16.2 nM) and ionomycin (1 μM), and the nuclei were isolated as described previously (24, 25). Isolated nuclei were fixed in 4% paraformaldehyde and stained with DAPI, and EGFP fluorescence intensity of $DAPI^{+}$ events was assessed using flow cytometry.

Luciferase reporter gene assay

The Luciferase Reporter Gene Assay, High Sensitivity for determination of firefly luciferase activity was purchased from Roche. Reporter cells were stimulated for 7 h, and luciferase activity was measured using a Mithras LB940 multimode plate reader (Berthold, Bad Wildbad, Germany).

Cytokine measurement

Cell culture supernatants were analyzed using Luminex xMAP suspension array technology (Austin, TX). Standard curves were generated using rIL-2 (R&D Systems, Minneapolis, MN).

Pull-down experiments and mass spectrometry

Cells were lysed in lysis buffer (150 mM NaCl, 1 μM PMSF, 1 mM sodium orthovanadate, 50 mM NaF, 0.5% lauryl-maltoside, 1× protease inhibitor mixture, 50 mM HEPES [pH 7.5]). For pull-down of HA-tagged CD147 constructs, the lysate was incubated with agarose coated with anti-HA mAb (Sigma-Aldrich); for the endogenous CD147 pull-down, we used CNBr-activated Sepharose 4B beads (GE Healthcare, Little Chalfont, U.K.) coupled to CD147 mAb MEM-M6/4 or to isotype-control mAb AFP-01.

Mass spectrometry

For affinity purification–mass spectrometry (AP-MS) of Jurkat T cells, proteins were eluted from the beads using urea buffer (6 M urea, 2 M thiourea, 10 mM HEPES [pH 8]), digested with trypsin (Promega) and Lys-C (WAKO, Osaka, Japan), and analyzed using electrospray ionization–liquid chromatography–tandem MS, as described earlier (26). Data were analyzed using MaxQuant 1.3.6.1 software (27), the Andromeda search engine (28), and the Perseus data analysis tool (http://www.perseus-framework.org/).

The AP-MS samples of primary T cells were analyzed using a slightly different methodological approach. Proteins were precipitated using a methanol-chloroform procedure (29) and were digested tryptically, as previously described (30). Peptides were separated and analyzed in an LTQ Velos ion trap mass spectrometer (Thermo Fisher, Bremen, Germany). Peptides were separated using an UltiMate Plus Nano HPLC separation system consisting of a Famos autosampler, Switchos column switching unit, UltiMate nano pump, and a UV detector (LC Packings, Amsterdam, The Netherlands). An Acclaim C18 trap column (300 μm inner diameter × 5 mm) was used at ambient temperature, and the Acclaim C18 nano separation column (75 μm inner diameter × 250 mm) was mounted in the column oven and operated at 45°C. Samples were loaded onto the trap column using 0.1% trifluoroacetic acid at 30 μl/min, and nano separation was performed in gradient mode at 300 nl/min from 0.1 formic acid (FA) in 5% aqueous acetonitrile (AcN); 0.08% FA in 15% methanol, 15% AcN, 70% water; and 0.08% FA in 60% AcN, 30% methanol, and 10% 2,2,2-trifluoroethanol. A User-defined Injection Program was used for sample injection and additional injector and trap column wash. Samples were analyzed in an LTQ Velos ion trap mass spectrometer (Thermo Fisher, Bremen, Germany) with the Top 20 method. Singly charged ions were excluded from fragmentation, and detected ions were excluded for further fragmentation for 3 min after initial tandem MS fragmentation. Data were analyzed using Mascot 2.4.1 software (Matrix Science, London, U.K.), searching in the most recent version of the Swiss-Prot database with a mass tolerance of 0.4 Da for mass spectrometry (MS) and tandem MS. Identifications with two peptides/protein and a Mascot score > 40 were accepted.

Data were analyzed using Mascot 2.4.1 software (Matrix Science), the SwissProt database, Scaffold 3.6.2 software (http://www.proteomesoftware.com), and Perseus.

The MS proteomics data were submitted to the ProteomeXchange Consortium (31) via the PRIDE partner repository with the dataset identifier PXD003029 and 10.6019/PXD003029 (http://www.ebi.ac.uk/pride/archive/).

Surface biotinylation and surface protein pull-down

Cells were surface biotinylated with 0.5 mg/ml EZ-Link Sulfo-NHS-SS-Biotin (Thermo Scientific, Rockford, IL) in PBS, according to the manufacturer's protocol, and lysed in lysis buffer (150 mM NaCl, 1% Brij-58 [Thermo Scientific], 1× protease inhibitor mixture, 50 mM HEPES [pH 7.5]), and the lysate was incubated for 2 h with high-performance streptavidin Sepharose (GE Healthcare). The supernatant (pull-down supernatant) was harvested, and the biotinylated surface molecule pull-down (pull-down) was eluted using Laemmli buffer.

Density gradient centrifugation

Cells were either left unstimulated or stimulated for 5 min with 2 μg/ml OKT3 plus 1 μg/ml Leu-28. The cells were lysed in 200 μl 1% Brij-58, 150 mM NaCl, 1× protease inhibitor mixture, 20 mM Tris-HCl (pH 7.5). The lysate was mixed 1:1 with 80% sucrose, 150 mM NaCl, 20 mM Tris-HCl (pH 7.5) and transferred to an 11 × 34-mm ultracentrifuge tube (Beckman Coulter, Brea, CA). A gradient was built by adding 1200 μl 30% sucrose and 400 μl 5% sucrose in 150 mM NaCl, 20 mM Tris-HCl (pH 7.5). The gradient was centrifuged at 137,000 × *g* for 16 h at 4°C in a Sorvall RC-M150GX Micro-Ultracentrifuge (Thermo Scientific, Waltham, MA). Subsequently, 10 200-μl fractions were taken from the top to the bottom.

Immunoblotting

Western blot analysis was performed as documented earlier (32).

Statistics

For statistical analysis we used the unpaired Student *t* test with the Welch correction. All experiments were done at least in triplicate and, unless stated otherwise, are representative of at least three independent experiments.

The significance of the MS results was analyzed using the Perseus software package 1.5.2.6 (http://www.perseus-framework.org/), with significance analysis of microarrays accounting for the permutation-based false discovery rate (FDR) and the size of the effect (parameters: FDR ≤ 0.05, S0 = 2). Thereby the q-value from permutation-based FDR calculations (33) and the test statistic (34) were calculated for each protein (Supplemental Tables I, II). A threshold for significant interaction partners was set to an FDR ≤ 0.05. In addition, the *p* value calculated using a two-tailed unpaired Student *t* test with equal variances and the difference of logarithmized mean expression values is given for each protein. A volcano plot depicts the *p* value (*y*-axis) and the difference (*x*-axis); the threshold for the significant area in the plot is shown as a parabola.

Results

Silencing of CD147 in T cells increases IL-2 production without affecting early TCR signaling

To study the immunomodulatory role of CD147 in T cells, we silenced CD147 in Jurkat and primary human T cells by lentiviral shRNA–mediated gene knockdown. The silencing efficiency was assessed using qPCR, cell surface immunofluorescence staining, and flow cytometry analysis. Upon silencing of CD147, mRNA levels were reduced by 70% (Fig. 1A) and 85% (Fig. 1D) in primary T cells and Jurkat T cells, respectively, which resulted in the reduction of CD147 surface expression by ~30% in primary T cells (Fig. 1B) and 80% in Jurkat T cells (Fig. 1E) compared with cells transduced with a nontargeting shControl.

Silencing of CD147 in primary T cells enhanced IL-2 production upon stimulation with CD3 and CD28 mAbs up to seven times

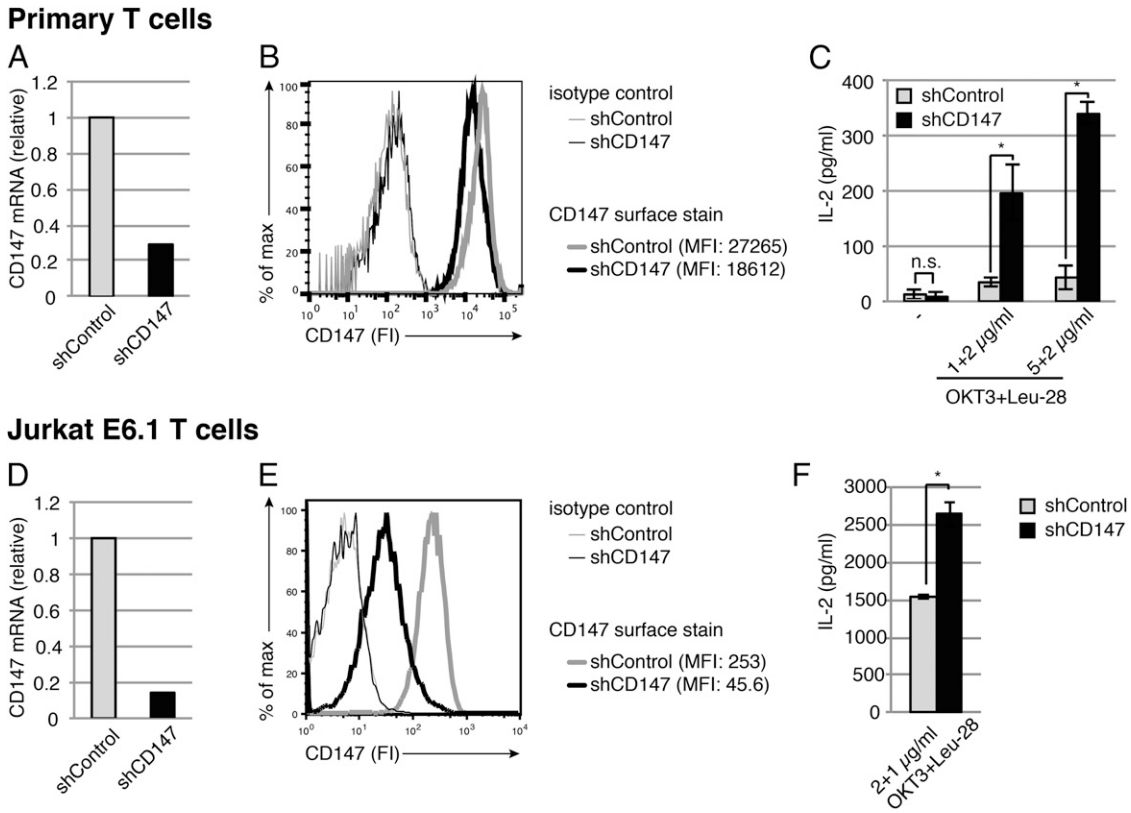

FIGURE 1. CD147 silencing enhances IL-2 production in primary and Jurkat T cells. The silencing efficiency of CD147 in primary T cells (**A**) and Jurkat E6.1 T cells (**D**) expressing an shRNA construct for silencing CD147 (shCD147) or a nontarget shControl was tested by qPCR. Silenced and shControl primary T cells (**B**) and Jurkat T cells (**E**) were surface labeled using CD147 mAb MEM-M6/1 or isotype-control mAb AFP-01 and analyzed using flow cytometry. Mean fluorescence intensity (MFI) is given for CD147 staining. (**C**) CD147-silenced primary T cells were stimulated with different concentrations of plate-bound CD3 mAb OKT3 plus soluble CD28 mAb Leu-28. After 24 h, supernatants were harvested, and IL-2 concentration was determined by Luminex assay. (**F**) IL-2 concentration in the supernatants of Jurkat T cells stimulated for 18 h with OKT-3 (2 μg/ml) plus Leu-28 (1 μg/ml). One representative experiment from two (A, C, and D), three (B and F), or five (E) experiments is shown, and the mean and SE were calculated from triplicates. $*p < 0.05$, Welch t test. n.s., not significant.

compared to the shControl levels (Fig. 1C); production nearly doubled in Jurkat T cells (Fig. 1F). The enhanced IL-2 production following silencing of CD147 was due to increased activity of the IL-2 promoter, irrespective of the stimulus used (SEE-pulsed Raji B cells [Fig. 2A] or CD3 mAb OKT3 plus CD28 mAb Leu-28 [Fig. 2B]). Notably, we also observed enhanced IL-2 promoter activity and protein production in CD147-silenced cells when we bypassed early TCR signaling with the PKC activator PMA and the calcium ionophore ionomycin (Fig. 2C, 2D). These data indicate that the immunomodulatory function of CD147 acts downstream of calcium mobilization. To test this hypothesis, we analyzed the impact on activating phosphorylation sites of early TCR signaling components (i.e., lymphocyte protein tyrosine kinase Lck [Y394] and PLCγ [Y783]) and found that they were not augmented by CD147 silencing (Fig. 2E, Supplemental Fig. 1A). Nevertheless, the downstream targets of PKC and PLCγ, the transcription factors NF-κB (Fig. 2F) and NFAT (Fig. 2G), displayed considerably more transcriptional activity in CD147-silenced cells. In addition, using an NFAT-EGFP–transgenic cell line and analyzing isolated nuclei by flow cytometry (for the scheme and experimental proof of concept see Supplemental Fig. 1B), we found that nuclei displayed 1.5-fold more NFAT-EGFP in CD147-silenced cells compared with shControl nuclei (Fig. 2H).

The cytoplasmic domain of CD147 is dispensable for its immunomodulatory role

To define signaling pathways that link CD147 with IL-2 promoter activity, we aimed to identify the immunomodulatory portion of CD147. We generated an RNA interference (RNAi)-resistant CD147 construct and used it as a basis for stepwise truncations and chimeric swap mutants (for detailed illustration and mutant names see Fig. 3A). An IRES-GFP–containing retroviral expression vector allowed assessment of transduction efficiency.

To exchange endogenous CD147 with our CD147 constructs, we coexpressed the RNAi-resistant mutants in combination with CD147 shRNA in Jurkat T cells. Cell surface staining with the CD147 mAbs MEM-M6/1 or MEM-M6/6 targeting the IgI or IgII domains of CD147, respectively, together with flow cytometry analysis (Fig. 3B), showed that we could rescue surface expression levels of CD147 with the full-length CD147 construct in CD147-silenced cells. Of note, all constructs showed different surface expression levels. The constructs containing the CD7 transmembrane domain (CD147e, CD147c) showed up to 10-fold higher expression on the cell surface than did constructs containing the CD147 transmembrane domain (CD147etc, CD147et, CD147IgIIt, CD147IgIt, CD147tc). A lack of the cytoplasmic domain of CD147 (CD147et, CD147IgIIt) slightly reduced surface expression levels compared with the full-length construct. However, the construct CD147IgIt, lacking the cytoplasmic domain and the IgII domain, was basically not expressed on the cell surface, indicating that the main determinants for surface expression are located in the IgII domain of CD147. Notably, the CD147IgIIt and CD147tc transfectants, both devoid of the IgI domain, showed decreased surface staining with mAb MEM-M6/1. Because the MEM-M6/1 epitope is located in the IgI domain, the MEM-M6/1 signal in these transfectants can originate only from the residual endogenous

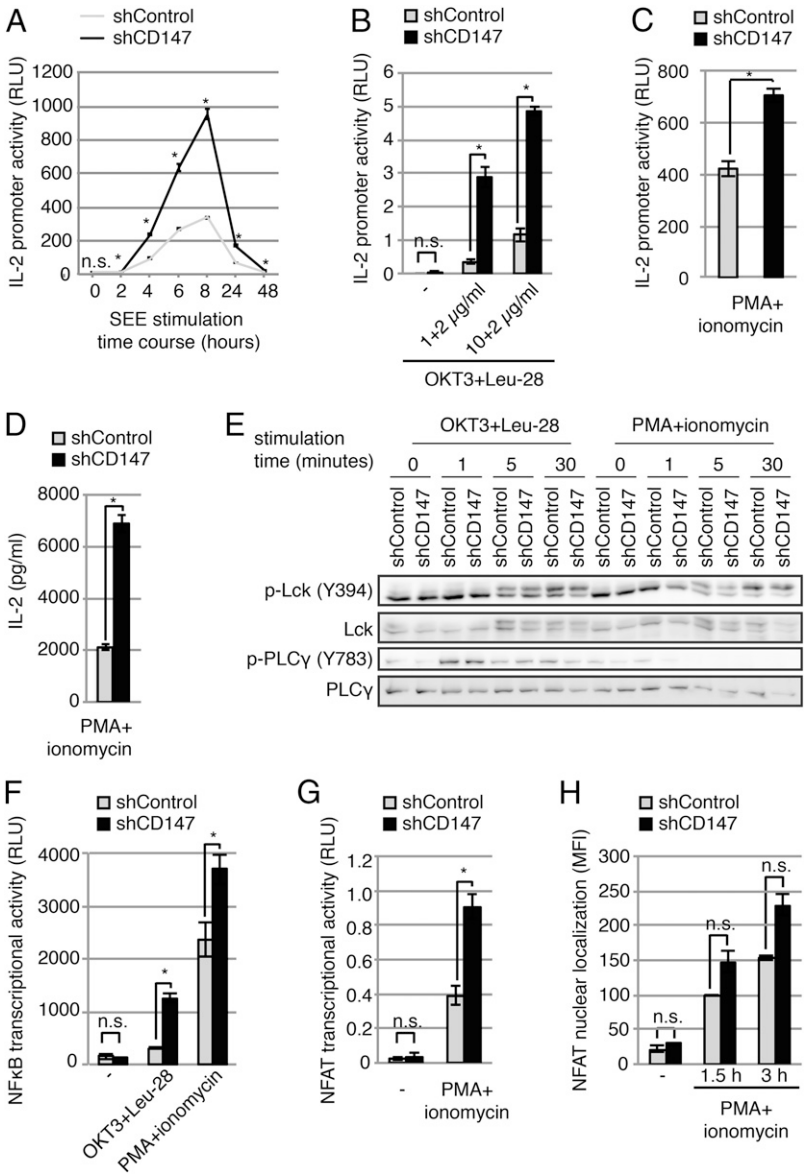

FIGURE 2. Analysis of TCR/CD3 and CD28 signaling pathways in CD147-silenced cells. (**A**) Jurkat T cells expressing luciferase under the control of the IL-2 promoter were silenced with CD147-specific shRNA or the shControl construct. Cells were stimulated for the indicated time intervals with Raji B cells pulsed with 10 ng/ml SEE; relative light units (RLU) of luciferase activity were measured on a multimode plate reader. (**B** and **C**) Cells from (A) were stimulated for 6 h, as indicated, and IL-2 promoter activity was assessed as in (A). (**D**) IL-2 protein levels in supernatants from silenced Jurkat T cells stimulated for 8 h with PMA (16.2 nM) plus ionomycin (1 μM) were determined by Luminex assay. (**E**) CD147-silenced and shControl Jurkat T cells were stimulated for 0, 1, 5, and 30 min at 37°C with mAb OKT3 (2 μg/ml) plus Leu-28 (1 μg/ml) or with PMA (16.2 nM) plus ionomycin (1 μM). Cells were lysed, and the lysates were analyzed with the indicated Abs by Western blotting. (**F**) NF-κB transcriptional activity was tested with an NF-κB reporter gene technique using the Jurkat T cell clone NF-κB–Luc. CD147-silenced and shControl NF-κB–Luc Jurkat T cells were stimulated for 8 h with OKT3 (1 μg/ml) plus Leu-28 (0.5 μg/ml) or PMA (16.2 nM) plus ionomycin (1 μM); relative light units (RLU) were assessed. (**G**) NFAT transcriptional activity was analyzed with the reporter gene technique using the Jurkat T cell clone NFAT-Luc. CD147-silenced or shControl Jurkat NFAT-Luc T cells were stimulated for 6 h with PMA plus ionomycin, and RLU were determined. One representative experiment from two (A and F), three (B and E), or five (C, D, and G) experiments is shown, and the mean ± SE was calculated from triplicates. (**H**) Flow cytometry was used to monitor NFAT nuclear translocation in isolated nuclei. shCD147 and shControl Jurkat T cells expressing NFAT-GFP were stimulated for the indicated time periods with PMA plus ionomycin; GFP content of the isolated DAPI$^+$ nuclei was analyzed using flow cytometry. Mean fluorescence intensity (MFI) and SE of independent experiments ($n = 3$) are given. *$p < 0.05$, Welch t test. n.s., not significant.

CD147. In contrast, the transfectant CD147c, which differs from CD147tc only in exchange of the CD147 transmembrane domain, did not reduce surface levels of endogenous CD147. The single-cell analysis revealed that the downregulation of endogenous CD147 correlated negatively with the expression of CD147IgIIt or CD147tc (Fig. 3B). Thus, the amount of CD147 on the cell surface is obviously controlled by molecular interactions at its transmembrane domain.

To test the effect of these constructs on PMA plus ionomycin–stimulated IL-2 production, we gated GFP^{high} cells and used intracellular immunofluorescence staining and flow cytometry to measure the percentage of IL-2–producing cells. As shown in Fig. 3C, the full-length RNAi-resistant construct CD147etc rescued the phenotype, reducing the numbers of IL-2$^+$ cells in CD147-silenced cells to shControl levels. A significant rescue of phenotype was also found with the constructs containing the CD147 IgII domain together with the CD147 transmembrane domain (CD147et and CD147IgIIt), whereas all other constructs failed. Thus, the transmembrane domain in conjunction with the IgII domain of CD147, or at least their interface, is important for the immunomodulatory function of CD147.

Identification of CD147 domain-specific interaction partners by MS

Having mapped the immunomodulatory portion of CD147, we aimed to identify the domain-specific functional interaction partners of CD147. We tagged full-length CD147, the minimal functional construct CD147IgIIt, and the nonfunctional constructs CD147e and CD147IgIt with an HA tag downstream of the signal sequence. This tag did not affect the immunomodulatory capacity of CD147 (Supplemental Fig. 2A). Consistent with the nontagged constructs, the surface expression varied among the HA-tagged constructs. The CD147IgIt construct was not detected in HA surface staining (Supplemental Fig. 2B); however, immunoblotting with the conformation-specific CD147 mAb MEM-M6/1 and the HA mAb recognized an unglycosylated variant of this construct (Supplemental Fig. 2C). This indicated intracellular expression of the CD147IgIt construct.

HA pull-down experiments and subsequent MS analysis of lysates from Jurkat T cells expressing the above-described constructs allowed identification of domain-specific interaction partners of CD147. We performed label-free quantification of protein intensities from AP-MS experiments and determined significant interaction

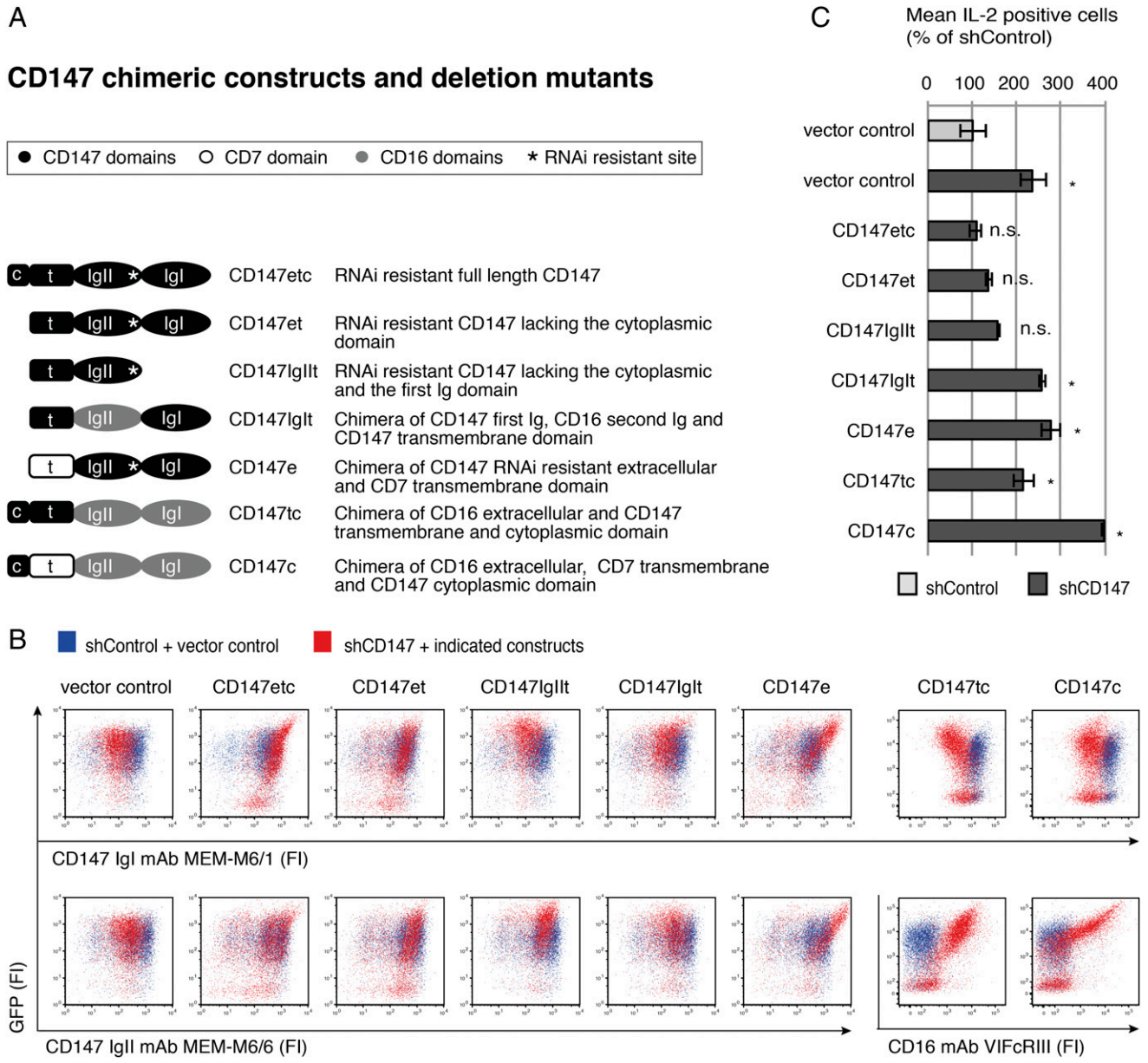

FIGURE 3. Defining the immunomodulatory portion of CD147. (**A**) Schematic illustration of the RNAi-resistant mutants. The cytoplasmic, transmembrane, whole extracellular, and extracellular Ig-like domains II and I are indicated by c, t, e, IgII, and IgI, respectively. CD147 domains are shown in black, the CD7 transmembrane domain (CD7t) is shown in white with a black outline, and the CD16 Ig-like domains II and I (CD16IgII, CD16IgI) are in gray. The asterisk in CD147etc, CD147et, CD147IgIIt, and CD147e indicates the RNAi-resistant site. The short name used in all subsequent figures is shown to the *right* of the illustration. The last column describes in detail the RNAi-resistant constructs. (**B**) Surface expression levels of the RNAi-resistant mutants. CD147-silenced (red) and shControl (blue) Jurkat T cells were transduced with the CD147 RNAi-resistant mutants cloned in an IRES-GFP vector or the vector control, respectively. Cells were surface labeled with mAbs recognizing the CD147 IgI domain (MEM-M6/1), CD147 IgII domain (MEM-M6/6), or CD16 IgI domain (VIFcRIII) and analyzed using flow cytometry. The dot plot overlay of shCD147 and shControl cells correlates cell surface staining by the mAbs (*x*-axis) with IRES-mediated GFP expression (*y*-axis). (**C**) Intracellular IL-2 levels of cells expressing the RNAi-resistant mutants. After 6 h of stimulation with PMA (16.2 nM) plus ionomycin (1 μM), cells were stained intracellularly for IL-2 and analyzed using flow cytometry. GFP^{high} cells were gated, and the percentages of $IL\text{-}2^{+}$ cells were measured. Data were normalized to the values of shControl/empty vector control cells. (B and C) One representative experiment from three independent experiments is shown, and the mean and SE were calculated from triplicates. $*p < 0.05$, shControl/empty vector control versus other cells, Welch *t* test. n.s., not significant.

partners using a permutation-based FDR calculation on the *t* test results (q-values) (Perseus software package 1.5.2.6, http://www.perseus-framework.org/). Interaction partners were identified based on the reproducibility of their enrichment with the bait (*p* value; *y*-axis in the volcano plot) and their fold enrichment compared with the control pull-down (difference; *x*-axis in the volcano plot). The result of pairwise statistics from all identified proteins and experimental approaches is provided (Supplemental Tables I, II).

We identified proteins significantly enriched in the specific full-length CD147 pull-downs by comparing the values with the negative control (i.e., cells expressing no HA tag). The significantly enriched proteins are those with q-values ≤ 0.05 (shown in Fig. 4 on the *right side* of the parabola in the volcano plot and listed in the table). Among them are the already-described interaction partners of CD147: monocarboxylate transporter 1 (SLC16A1) (35–37), amino acid transporter CD98 H chain (CD98, SLC3A2) (35, 38),

Na(+)/K(+) ATPase α-1 subunit (35), and MHC class I A (HLA-A) (35). Of note, we also identified previously unknown interactions of CD147 with plasma membrane calcium ATPase isoform 4 (PMCA4, ATP2B4) and moesin (denoted by bold type in Fig. 4A).

To restrict the identified interaction partners of CD147 to those interacting with the immunomodulatory portion, we used comparative MS analysis of the full-length HA-construct CD147etc with the minimal functional (CD147IgIIt) and nonfunctional (CD147e, CD147IgIt) HA-tagged mutants. Using pairwise comparisons, we confirmed that the interaction of MCT1 with CD147 depended on the cytoplasmic tail of CD147 (36, 37), because it was enriched with full-length CD147 but not with the constructs lacking the intracellular domain (difference $>$ 4 when comparing HACD147etc with the other constructs, Fig. 5A–C, Supplemental Fig. 2D, Supplemental Table I). In contrast, the plasma membrane calcium exporter PMCA4 and amino acid transporter H chain CD98 showed a very large difference when comparing the nonfunctional constructs HACD147e and HACD147IgIt with the full-length construct HACD147etc (difference[PMCA4] = 4.1 and 4.7; difference[CD98] = 3.1 and 4.1) but not when comparing the minimal functional construct HACD147IgIIt with HACD147etc (difference[PMCA4] = 0.6; difference[CD98] = 1.3) (shown in the *left shift* in Fig. 5A compared with Fig. 5B and 5C, Supplemental Fig. 2D, Supplemental Table I). This indicated that the associations with PMCA4 and CD98 were independent of the cytoplasmic domain but required the IgII and transmembrane domains. To validate the association of PMCA4 with the minimal functional construct HACD147IgIIt in Jurkat T cells, we analyzed the respective CD147 pull-downs for the presence of PMCA4 by immunoblotting (Fig. 5D).

We confirmed the interaction of endogenous CD147 with MCT1 and PMCA4 in primary human T cells using AP-MS analysis and found monocarboxylate transporter 4, keratin (K2C6B), hexokinase-1, and ubiquitin 60S ribosomal protein L40 as additional interaction partners in these cells (Fig. 5E). In addition, we tested the interaction of PMCA4 with endogenous CD147 in primary T cells by analyzing the CD147 pull-down by immunoblotting (Fig. 5F).

Cell surface expression of PMCA4 is independent of CD147, whereas calcium-mobilization dynamics are affected by CD147

Previous studies showed that CD147 shuttles the transporter molecules MCT1, MCT4 (37), and CD98 (35) to the plasma membrane and stabilizes their surface expression, which is necessary for their proper function. We tested the impact of CD147 on the surface expression level of PMCA4 using surface biotinylation of shCD147 and shControl Jurkat T cells, purification of biotinylated surface molecules with streptavidin-coated beads, and analysis by Western blotting (Supplemental Fig. 3A). As shown in Fig. 6A and 6B, CD147 silencing did not affect plasma membrane–expressed PMCA4 (SA pull-down). In addition to its shuttling function to the plasma membrane, we showed previously that CD147 influenced the lipid raft localization of CD48 and CD59 (14). However, density gradient centrifugation with CD147-silenced cells, stimulated or not with OKT3 plus Leu-28, showed that silencing of CD147 did not change the distribution of PMCA4 from the nonraft to the lipid raft compartment (Fig. 6C, Supplemental Fig. 3B).

PMCA4 serves as a plasma membrane calcium exporter, which contributes to re-establishment of homeostatic intracellular calcium levels after calcium mobilization (reviewed in Ref. 39). To determine whether CD147 and PMCA4 are involved in calcium homeostasis during T cell stimulation, we compared the calcium dynamics of CD147- and PMCA4-silenced cells. We silenced PMCA4 in Jurkat T cells with two shRNAs (shPMCA4_P1 and shPMCA4_P2) and used the nonfunctional construct shPMCA1_P1 targeting the plasma membrane calcium ATPase isoform 1 as a negative control (Supplemental Fig. 3C). Silencing of PMCA4 reduced mRNA levels by 70% (Supplemental Fig. 3D) and protein levels by 30–40% (Fig. 6D) compared with cells transduced with a nontargeting shRNA control. Next, we used flow cytometry to analyze the changes in cytosolic calcium levels following CD3 plus CD28 stimulation (Fig. 6E, *upper panels*) or PMA plus ionomycin

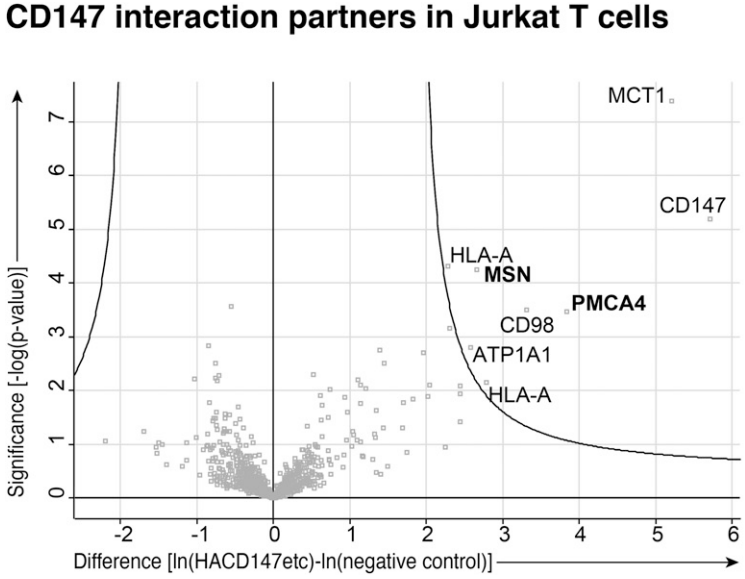

	p-value [-log10]	q-value	difference [ln]	test statistic
CD147	5.19	0.00	5.72	2.24
MCT1	7.39	0.00	5.21	2.30
PMCA4	3.47	0.00	3.84	1.45
CD98	3.50	0.00	3.31	1.30
HLA-A	2.15	0.05	2.78	1.00
MSN	4.26	0.02	2.66	1.13
ATP1A1	2.80	0.05	2.58	1.01
HLA-A	4.31	0.04	2.28	0.99

FIGURE 4. CD147 interaction partners in Jurkat T cells. HA pull-down experiments, followed by liquid chromatography–tandem MS analysis, were performed with cells expressing HA-tagged CD147 and wild-type Jurkat T cells, which served as a negative control. Proteins coprecipitated with HA-tagged CD147 in five independent experiments were analyzed for significant enrichment compared with the negative control using significance analysis of microarrays in the Perseus software package (parameters: FDR $\leq$ 0.05, S0 = 2). Significant hits are shown in the volcano plot on the *right side* of the parabola. Significance based on the Student *t* test is given as the logarithm to the base 10 of the *p* value (*y*-axis). The *x*-axis shows enrichment of interaction partners in the HACD147etc pull-down compared with the negative control, depicted as the natural logarithm from normalized intensity values. The highly significant interaction partners, determined using Perseus, are labeled. The newly identified interaction partners are in bold type.

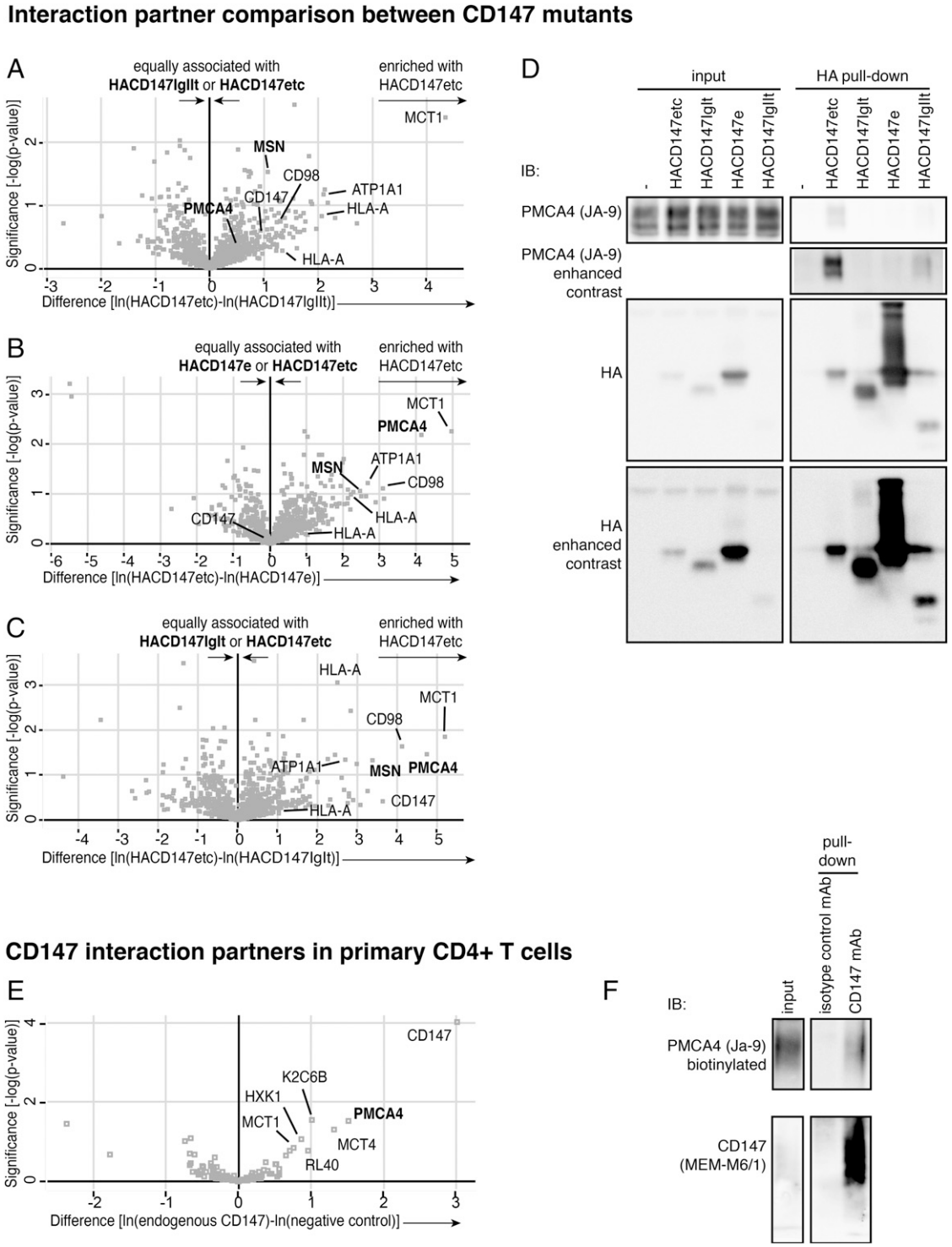

FIGURE 5. PMCA4 interacts with the immunomodulatory portion of CD147 in Jurkat T cells and in primary T cells. Jurkat T cells expressing the indicated constructs were used in comparative HA pull-down experiments, followed by MS analysis. Three independent experiments (**A** and **B**) or two independent experiments (**C**) were used to test the significance of construct-specific interactions with the Perseus program and are shown in a volcano plot, as in Fig. 4. For convenience, only the highly significant interaction partners defined in Fig. 4 are labeled. Interaction partners of full-length CD147 (HACD147etc) were compared with the minimal functional mutant (HACD147IgIIt) or the nonfunctional mutants (A), HACD147e (B), or HACD147IgIt (C). The newly identified interaction partners are in bold type. The complete statistical analysis from pairwise comparisons of all identified proteins is shown in Supplemental Table I. (**D**) Western blot analysis of pull-down of HA-tagged CD147 mutants expressed in Jurkat T cells with indicated mAbs. One representative Western blot from two independent ones is shown. Input shows lysate cleared from insoluble particles by centrifugation, before pull-down was performed; HA pull-down shows specifically enriched molecules. (**E**) AP-MS of endogenous CD147 from lysates of primary T cells. The volcano plot shows the pull-down of endogenous CD147 with mAb MEM-M6/4 compared with that of the isotype control (mAb AFP-01) from four independent experiments. Highly significant interaction partners from Fig. 4, and hits in between, are labeled. The complete statistical analysis is shown in Supplemental Table II. (**F**) Western blot analysis of endogenous CD147 pull-down from lysates of primary T cells with indicated mAbs. One representative Western blot from two independent ones is shown.

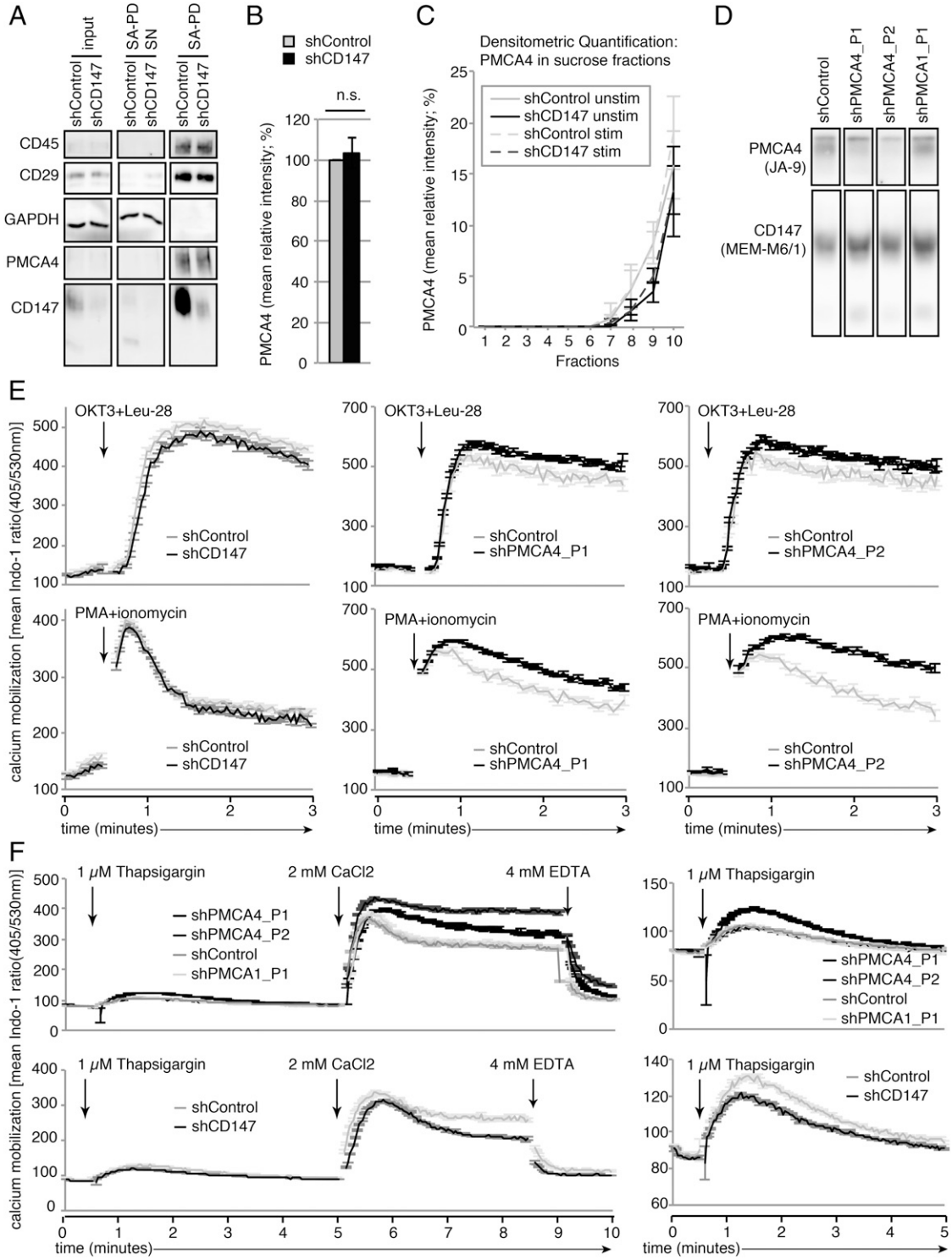

FIGURE 6. Plasma membrane localization of PMCA4 and calcium-mobilization kinetics in PMCA4- and CD147-silenced cells. (**A**) Surface biotinylation and pull-down of biotinylated plasma membrane–associated molecules by streptavidin Sepharose using CD147-silenced and shControl Jurkat T cells. Isolated fractions: the input, streptavidin pull-down supernatant (SA-PD SN), and streptavidin pull-down (SA-PD) were analyzed using Western blotting for the presence of indicated proteins. One representative blot from four independent experiments is shown. (**B**) Statistical evaluation of the relative intensity of PMCA4 signals from the streptavidin pull-down fraction of four independent experiments. Welch *t* test. (**C**) Membrane fractionation of CD147-silenced and shControl Jurkat T cells by sucrose density gradient centrifugation. Cells were left unstimulated or were stimulated with 2 μg/ml OKT3 plus 1 μg/ml Leu-28 for 5 min at 37°C and 5% CO_2 before they were lysed and subjected to membrane fractionation by ultracentrifugation. Densitometric analysis of immunoblots from three independent density gradient centrifugation experiments is shown. The mean and SE are shown for the respective fraction; statistical analysis (Welch *t* test) found no significant differences between shControl and CD147-silenced cells. (**D**) Jurkat T cells were silenced for PMCA4 with two shRNA constructs (P1, P2). The constructs shPMCA1_P1 and shControl were used as negative controls. Silencing efficiency of PMCA4 was estimated at the protein level using Western blotting with the indicated mAbs. One representative blot from three independent experiments is shown. (**E**) Flow cytometry analysis of calcium-mobilization dynamics following treatment of PMCA4- or CD147-silenced and shControl Jurkat T cells with T cell–stimulating agents. The traces show mean Indo-1 ratio (405/530) from 100–1000 cells/time point and SE from one (*Figure legend continues*)

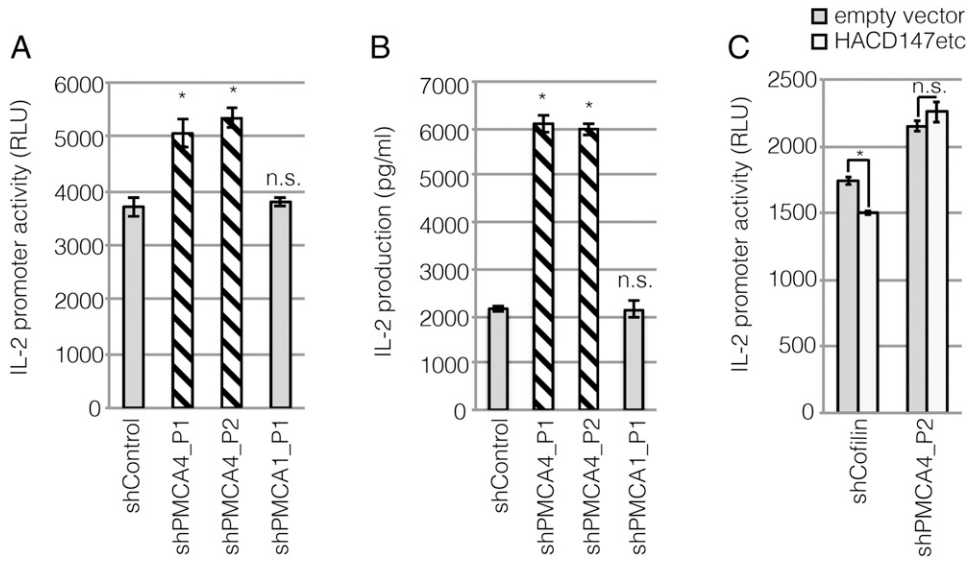

FIGURE 7. PMCA4 is essential for the immunomodulatory function of CD147. (**A**) PMCA4-silenced Jurkat T cells expressing a luciferase gene under the control of the IL-2 promoter were treated for 12 h with PMA plus ionomycin. IL-2 promoter activity, given as relative light units (RLU), was determined. One representative experiment from five independent experiments is shown. (**B**) PMCA4-silenced cells were stimulated for 12 h with PMA plus ionomycin, and the supernatant concentration of IL-2 was measured by Luminex assay. One representative experiment from three independent experiments is shown. (**C**) PMCA4- or cofilin-silenced Jurkat IL-2–Luc reporter cells overexpressing HACD147etc or containing an empty vector control were stimulated with PMA plus ionomycin for 7 h, and IL-2 promoter activity was assessed. One representative experiment from two independent experiments is shown. The mean and SE were calculated from triplicates, and significant differences between silenced cells and shControl cells (A and B) and between HACD147etc and the empty vector control (C) were determined. $*p < 0.05$, Welch t test. n.s., not significant.

treatment (Fig. 6E, *lower panels*). To control for artifacts resulting from differential handling of the silenced and shControl cells, one of the cell types was color coded and then the cells were pooled into a single tube for loading with the calcium-sensitive dye Indo-1 and subsequent stimulation and measurement. Silencing of PMCA4 (PMCA4_P1, PMCA4_P2) led to increased accumulation of intracellular calcium upon activation compared with shControl cells, and it was independent of the mode of stimulation. Strikingly, CD147 knockdown resulted in the opposite phenotype (i.e., a slight reduction in intracellular calcium levels). Nevertheless, statistical evaluation of the area under the curve showed that even the slight reduction following PMA plus ionomycin stimulation was statistically significant (Supplemental Fig. 3E). Previous studies showed that CD147 positively influences the release of calcium from internal stores (40), which prompted us to test this scenario with the CD147- and PMCA4-silenced cells. We began the intracellular calcium measurements in calcium-free buffer conditions and inhibited the sarcoplasmic/ER calcium ATPase with thapsigargin, resulting in calcium release from the ER. Notably, PMCA4_P1- and CD147-silenced cells showed opposite calcium-release dynamics from the ER; greater intracellular calcium was detected in PMCA4_P1-silenced cells, whereas CD147-silenced cells had lower levels (Fig. 6F, *right panels*). Further, in PMCA4-silenced cells, the addition of extracellular calcium resulted in increased intracellular calcium levels and delayed export following extracellular calcium chelation with EDTA; CD147-silenced cells showed a distinctive opposite trend (Fig. 6F, *left panels*). Therefore, we conclude that CD147 does not inhibit, but rather enhances, intracellular calcium levels following treatment with T cell–stimulating agents and that the inhibition of NFAT and NF-κB by CD147 is mediated independently of calcium mobilization.

The presence of PMCA4 is essential for immunomodulation by CD147

Silencing of CD147 did not change the surface expression of PMCA4 or target PMCA4 to lipid raft compartments; however, it decreased calcium levels, suggesting, paradoxically (in respect to the enhanced IL-2 production following silencing of CD147), a blocking effect on the calcium export of PMCA4. Thus, we next tested whether PMCA4 might be involved in the immunomodulatory function of CD147. Silencing of PMCA4 (Fig. 6D, Supplemental Fig. 3D), consistent with the enhanced calcium levels (Fig. 6E), augmented IL-2 promoter activity (Fig. 7A) and, consequently, increased IL-2 production (Fig. 7B). To determine whether PMCA4 is involved in CD147-dependent inhibition of the IL-2 promoter, we overexpressed the full-length HA-tagged CD147 construct in control and PMCA4-silenced cells. Consistent with our previous data, CD147 overexpression reduced IL-2 promoter activity in the control cells, but CD147 lost its immunomodulatory function in the PMCA4-silenced cells (Fig. 7C). To summarize, interaction of transmembrane and the IgII domain of

representative experiment of two to five independent experiments. Cells were stimulated with OKT3 plus Leu-28 (*upper panels*) or were treated with PMA plus ionomycin (*lower panels*). Calcium traces of CD147-silenced cells (coded by surface labeling with CD147 mAb MEM-M6/4-AF647) and shControl cells were measured in one tube (*left panels*). Calcium traces of CFSE color-coded shControl cells and noncoded PMCA4-silenced cells were measured in one tube (*middle* and *right panels*). (**F**) Flow cytometry analysis of calcium-mobilization dynamics from the ER (thapsigargin) or import and export dynamics across the plasma membrane ($CaCl_2$, EDTA) of cells from (E). Cells were kept in calcium-free buffer and treated with thapsigargin, $CaCl_2$, and EDTA at the indicated time points. One representative experiment of three independent experiments is shown. PMCA4-silenced cells, shPMCA1 cells, and shControl cells (*upper panels*). Cells were measured in separate tubes. CD147-silenced cells and shControl cells (*lower panels*). Total measurement (*left panels*). Details of the first 5 min of the panels on the *left* (*right panels*). n.s., not significant.

CD147 with PMCA4 affects the IL-2 transcription factors NFAT and NF-κB by a calcium-independent mechanism (Fig. 8).

Discussion

Hyperactivation of the immune system lies at the center of many autoimmune and allergic diseases, and it is prevented by upregulation of immunosuppressive proteins following lymphocyte activation. Several negative regulatory mechanisms that keep the T cell response in homeostatic balance are ascribed to inhibitory coreceptors, such as CTLA-4, PD-1, TIM-3, B7-H1, and B7-1 (reviewed in Ref. 7).

In this study we demonstrate, in partial agreement with a previous study (15), that CD147 is an inhibitory receptor that dampens IL-2 production at the level of NFAT- and NF-κB–regulated transcription. We extend these recent findings by showing that the inhibitory signal of CD147 on IL-2 expression is bypassing early TCR signaling components. A recent publication also supports the finding that silencing of CD147 does not enhance the activating phosphorylation of early signaling components (41). Furthermore, we show that, although CD147 enhances cytoplasmic calcium after treatment with T cell–stimulating agents or with thapsigargin plus high extracellular calcium, CD147 negatively regulates IL-2 expression by interaction with PMCA4.

PMCA4 (ATP2B4, MXRA1, EC3.6.1.8) is associated with the immunomodulatory portion of CD147, which consists of the membrane proximal IgII domain and the transmembrane domain of CD147. Plasma membrane calcium exporters and sodium/calcium exchangers are major regulators of calcium homeostasis in human cells (42). Jurkat T cells predominantly express PMCA4 (43) but lack sodium calcium exporters (44). Consequently, we found that

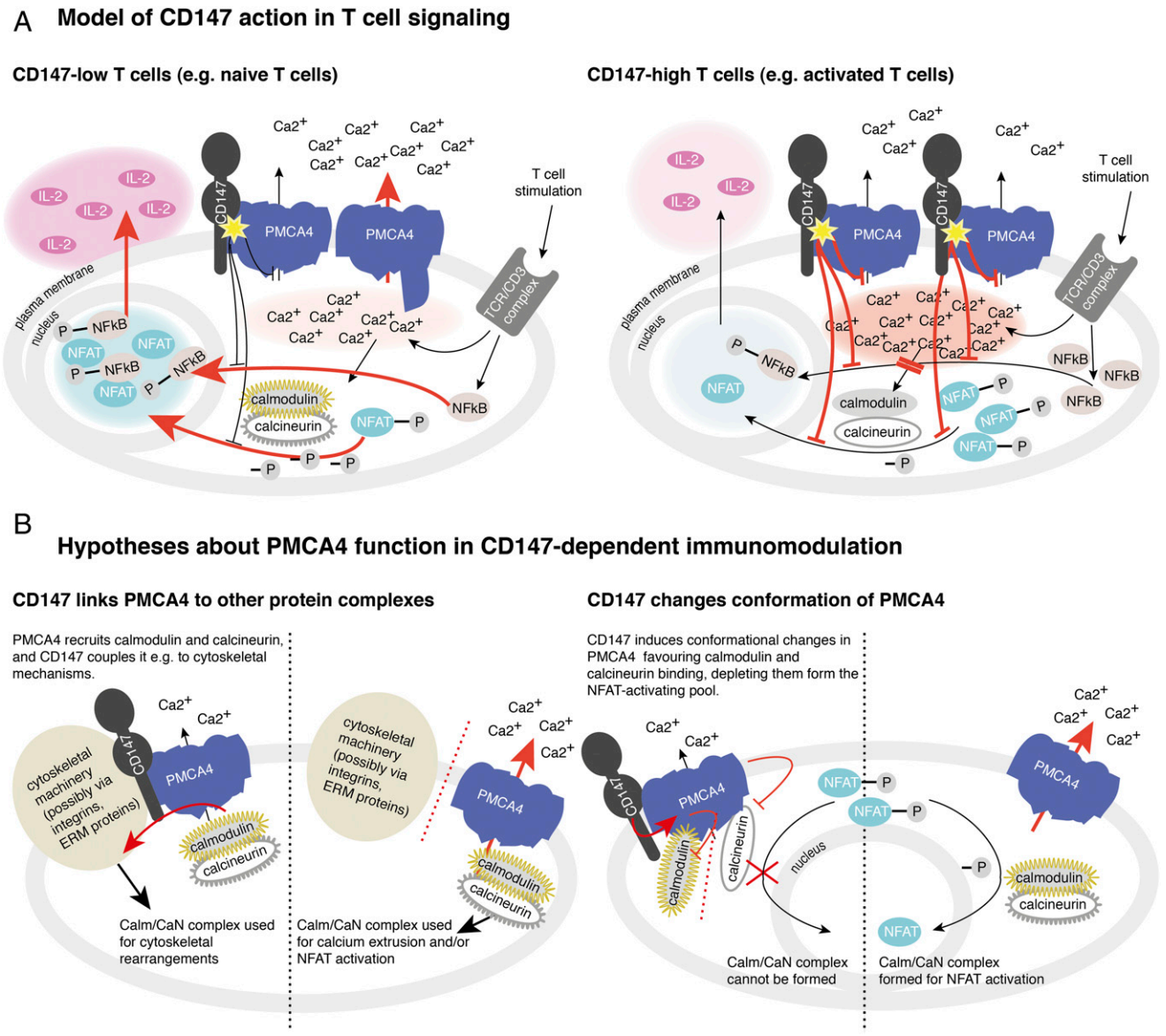

FIGURE 8. Model of the CD147/PMCA4 immunomodulatory complex and proposed hypotheses for its function. (**A**) Model of CD147 action in T cell signaling. In CD147^{low} cells, PMCA4 is more active, whereas the transcriptional activity of NFAT and NF-κB and subsequent IL-2 production are enhanced. In CD147^{high} cells, the interaction of PMCA4 with the immunomodulatory portion of CD147 affects PMCA4 calcium-exporting function but decouples the increased intracellular calcium level from activating NFAT and NF-κB. Red arrows and lines indicate enforced signal transduction. The attached P at the NF-κB or NFAT illustrates the different phosphorylation states in the cytosol and nucleus. (**B**) Hypotheses for the function of PMCA4 in immunomodulation of CD147. PMCA4 might work as an adaptor to attract and pass on calmodulin or calcineurin to other proteins in the proximity of CD147 (*left panel*). Alternatively, association of the CD147/PMCA4 complex with calmodulin or calcineurin might inhibit the NFAT-activating function of the calmodulin/calcineurin complex via a conformation change (*right panel*).

silencing of PMCA4 in Jurkat T cells affected calcium clearance, which was in agreement with previous observations (45). Although it was shown that CD147 acts as a transporter and stabilizer of cell surface expression of several molecules, including monocarboxylate and amino acid transporters (35, 37), silencing of CD147 did not reduce the level of surface-associated PMCA4. This, together with the finding that CD147 slows down the establishment of calcium homeostasis through the plasma membrane, indicates that CD147 might directly affect the calcium-exporting function of PMCA4 via an allosteric effect. However, the CD147-dependent inhibition of IL-2 promoter activity cannot be deduced from its potential inhibitory effect on the calcium-exporting function of PMCA4. PMCA4 was shown to interact with calmodulin (46) and calcineurin, and both regulate the activation of NFAT (reviewed in Ref. 3). In addition, calmodulin is involved in the activation of NF-κB (4–6). On the basis of these findings, and because we found that calmodulin is slightly enriched in the CD147 pull-down (Supplemental Table I) and that knockdown of PMCA4 blocks the inhibitory effect of CD147 on IL-2 promoter activity, we speculate that CD147 uses PMCA4 as an adaptor molecule acting on calmodulin. Thus, we hypothesize that CD147 either couples calmodulin and/or calcineurin via PMCA4 to other signaling events or it changes the conformation of PMCA4 and its affinity to calmodulin and/or calcineurin, thereby removing them from the transcription factor–activating calmodulin/calcineurin pool (Fig. 8B). Indeed, inhibition of the NFAT pathway by PMCA4, but not PMCA1, was recently ascribed to the association of calcineurin with PMCA4 (47). In this way, CD147 might affect the NFAT and NF-κB pathways in a calcium-independent fashion.

By this mechanism, low expression of CD147 in resting T cells could keep calcium homeostatically low, through reduced inhibition of PMCA4, while simultaneously providing basal expression of IL-2 for survival. Following activation of naive $CD147^{low}$ T cells, IL-2 production and T cell proliferation are promoted until the stimulation-dependent upregulation of the late activation marker CD147 (9) dampens IL-2 expression (Fig. 8A). One can further speculate that CD147 upregulated at a later stage (when T cells perform cytoskeletal rearrangements to enter tissue, to attack or act on other cells) decouples intracellular calcium signaling from gene expression (e.g., to allow calcium usage for migration, synaptic integrity, and transmission processes, which are functions of CD147 that were described in various cell types) (15, 18, 48–50).

Acknowledgments

We thank Eva Steinhuber (Institute for Hygiene and Applied Immunology, Medical University of Vienna), Margarethe Merio, and Petra Waidhofer-Söllner (Institute of Immunology, Medical University of Vienna) for excellent technical support; Reinhard Fässler (Department of Molecular Medicine, Max Planck Institute of Biochemistry) for experimental and intellectual support with MS analysis; and Thomas Baumruker, Michel J. Tremblay, Johannes Schmid, Vaclav Horejsi, Sheila Stewart, and Gary Nolan for providing materials specified in the *Materials and Methods* section.

Disclosures

The authors have no financial conflicts of interest.

References

1. Smith-Garvin, J. E., G. A. Koretzky, and M. S. Jordan. 2009. T cell activation. *Annu. Rev. Immunol.* 27: 591–619.
2. Vig, M., and J. P. Kinet. 2009. Calcium signaling in immune cells. *Nat. Immunol.* 10: 21–27.
3. Macian, F. 2005. NFAT proteins: key regulators of T-cell development and function. *Nat. Rev. Immunol.* 5: 472–484.
4. Hughes, K., A. Antonsson, and T. Grundstrøm. 1998. Calmodulin dependence of NFkappaB activation. *FEBS Lett.* 441: 132–136.
5. Jang, M. K., Y. H. Goo, Y. C. Sohn, Y. S. Kim, S. K. Lee, H. Kang, J. Cheong, and J. W. Lee. 2001. Ca2+/calmodulin-dependent protein kinase IV stimulates nuclear factor-kappa B transactivation via phosphorylation of the p65 subunit. *J. Biol. Chem.* 276: 20005–20010.
6. Hughes, K., S. Edin, A. Antonsson, and T. Grundström. 2001. Calmodulin-dependent kinase II mediates T cell receptor/CD3- and phorbol ester-induced activation of IkappaB kinase. *J. Biol. Chem.* 276: 36008–36013.
7. Chen, L., and D. B. Flies. 2013. Molecular mechanisms of T cell co-stimulation and co-inhibition. *Nat. Rev. Immunol.* 13: 227–242.
8. Perkins, D., Z. Wang, C. Donovan, H. He, D. Mark, G. Guan, Y. Wang, T. Walunas, J. Bluestone, J. Listman, and P. W. Finn. 1996. Regulation of CTLA-4 expression during T cell activation. *J. Immunol.* 156: 4154–4159.
9. Kasinrerk, W., E. Fiebiger, I. Stefanová, T. Baumruker, W. Knapp, and H. Stockinger. 1992. Human leukocyte activation antigen M6, a member of the Ig superfamily, is the species homologue of rat OX-47, mouse basigin, and chicken HT7 molecule. *J. Immunol.* 149: 847–854.
10. Igakura, T., K. Kadomatsu, O. Taguchi, H. Muramatsu, T. Kaname, T. Miyauchi, K. Yamamura, K. Arimura, and T. Muramatsu. 1996. Roles of basigin, a member of the immunoglobulin superfamily, in behavior as to an irritating odor, lymphocyte response, and blood-brain barrier. *Biochem. Biophys. Res. Commun.* 224: 33–36.
11. Koch, C., G. Staffler, R. Hüttinger, I. Hilgert, E. Prager, J. Cerný, P. Steinlein, O. Majdic, V. Horejsí, and H. Stockinger. 1999. T cell activation-associated epitopes of CD147 in regulation of the T cell response, and their definition by antibody affinity and antigen density. *Int. Immunol.* 11: 777–786.
12. Biegler, B., and W. Kasinrerk. 2012. Reduction of CD147 surface expression on primary T cells leads to enhanced cell proliferation. *Asian Pac. J. Allergy Immunol.* 30: 259–267.
13. Renno, T., A. Wilson, C. Dunkel, I. Coste, K. Maisnier-Patin, A. Benoit de Coignac, J. P. Aubry, R. K. Lees, J. Y. Bonnefoy, H. R. MacDonald, and J. F. Gauchat. 2002. A role for CD147 in thymic development. *J. Immunol.* 168: 4946–4950.
14. Staffler, G., A. Szekeres, G. J. Schütz, M. D. Säemann, E. Prager, M. Zeyda, K. Drbal, G. J. Zlabinger, T. M. Stulnig, and H. Stockinger. 2003. Selective inhibition of T cell activation via CD147 through novel modulation of lipid rafts. *J. Immunol.* 171: 1707–1714.
15. Ruiz, S., A. Castro-Castro, and X. R. Bustelo. 2008. CD147 inhibits the nuclear factor of activated T-cells by impairing Vav1 and Rac1 downstream signaling. *J. Biol. Chem.* 283: 5554–5566.
16. Solstad, T., S. J. Bains, J. Landskron, E. M. Aandahl, B. Thiede, K. Taskén, and K. M. Torgersen. 2011. CD147 (Basigin/Emmprin) identifies FoxP3+CD45RO+ CTLA4+-activated human regulatory T cells. *Blood* 118: 5141–5151.
17. Landskron, J., and K. Taskén. 2013. CD147 in regulatory T cells. *Cell. Immunol.* 282: 17–20.
18. Hu, J., N. Dang, H. Yao, Y. Li, H. Zhang, X. Yang, J. Xu, H. Bian, J. Xing, P. Zhu, and Z. Chen. 2010. Involvement of HAb18G/CD147 in T cell activation and immunological synapse formation. *J. Cell. Mol. Med.* 14: 2132–2143.
19. Forster, F., W. Paster, V. Supper, P. Schatzlmaier, S. Sunzenauer, N. Ostler, A. Saliba, P. Eckerstorfer, N. Britzen-Laurent, G. Schütz, et al. 2014. Guanylate binding protein 1-mediated interaction of T cell antigen receptor signaling with the cytoskeleton. *J. Immunol.* 192: 771–781.
20. Jursik, C., M. Prchal, R. Grillari-Voglauer, K. Drbal, E. Fuertbauer, H. Jungfer, W. H. Albert, E. Steinhuber, T. Hemetsberger, J. Grillari, et al. 2009. Large-scale production and characterization of novel CD4+ cytotoxic T cells with broad tumor specificity for immunotherapy. *Mol. Cancer Res.* 7: 339–353.
21. Paddison, P. J., J. M. Silva, D. S. Conklin, M. Schlabach, M. Li, S. Aruleba, V. Balija, A. O'Shaughnessy, L. Gnoj, K. Scobie, et al. 2004. A resource for large-scale RNA-interference-based screens in mammals. *Nature* 428: 427–431.
22. Muhammad, A., H. B. Schiller, F. Forster, P. Eckerstorfer, R. Geyeregger, V. Leksa, G. J. Zlabinger, M. Sibilia, A. Sonnleitner, W. Paster, and H. Stockinger. 2009. Sequential cooperation of CD2 and CD48 in the buildup of the early TCR signalosome. *J. Immunol.* 182: 7672–7680.
23. Bailey, S., and P. J. Macardle. 2006. A flow cytometric comparison of Indo-1 to fluo-3 and Fura Red excited with low power lasers for detecting Ca(2+) flux. *J. Immunol. Methods* 311: 220–225.
24. Poglitsch, M., K. Katholnig, M. D. Säemann, and T. Weichhart. 2011. Rapid isolation of nuclei from living immune cells by a single centrifugation through a multifunctional lysis gradient. *J. Immunol. Methods* 373: 167–173.
25. Schatzlmaier, P., V. Supper, L. Göschl, A. Zwirzitz, P. Eckerstorfer, W. Ellmeier, J. B. Huppa, and H. Stockinger. 2015. Rapid multiplex analysis of lipid raft components with single-cell resolution. *Sci. Signal.* 8: rs11.
26. Schiller, H. B., C. C. Friedel, C. Boulegue, and R. Fässler. 2011. Quantitative proteomics of the integrin adhesome show a myosin II-dependent recruitment of LIM domain proteins. *EMBO Rep.* 12: 259–266.
27. Cox, J., and M. Mann. 2008. MaxQuant enables high peptide identification rates, individualized p.p.b.-range mass accuracies and proteome-wide protein quantification. *Nat. Biotechnol.* 26: 1367–1372.
28. Cox, J., N. Neuhauser, A. Michalski, R. A. Scheltema, J. V. Olsen, and M. Mann. 2011. Andromeda: a peptide search engine integrated into the MaxQuant environment. *J. Proteome Res.* 10: 1794–1805.
29. Wessel, D., and U. I. Flügge. 1984. A method for the quantitative recovery of protein in dilute solution in the presence of detergents and lipids. *Anal. Biochem.* 138: 141–143.
30. Gregan, J., C. G. Riedel, M. Petronczki, L. Cipak, C. Rumpf, I. Poser, F. Buchholz, K. Mechtler, and K. Nasmyth. 2007. Tandem affinity purification of functional TAP-tagged proteins from human cells. *Nat. Protoc.* 2: 1145–1151.

31. Vizcaíno, J. A., E. W. Deutsch, R. Wang, A. Csordas, F. Reisinger, D. Ríos, J. A. Dianes, Z. Sun, T. Farrah, N. Bandeira, et al. 2014. ProteomeXchange provides globally coordinated proteomics data submission and dissemination. *Nat. Biotechnol.* 32: 223–226.
32. Leksa, V., R. Loewe, B. Binder, H. B. Schiller, P. Eckerstorfer, F. Forster, A. Soler-Cardona, G. Ondrovicová, E. Kutejová, E. Steinhuber, et al. 2011. Soluble M6P/IGF2R released by TACE controls angiogenesis via blocking plasminogen activation. *Circ. Res.* 108: 676–685.
33. Storey, J. D., and R. Tibshirani. 2003. Statistical significance for genomewide studies. *Proc. Natl. Acad. Sci. USA* 100: 9440–9445.
34. Tusher, V. G., R. Tibshirani, and G. Chu. 2001. Significance analysis of microarrays applied to the ionizing radiation response. *Proc. Natl. Acad. Sci. USA* 98: 5116–5121.
35. Xu, D., and M. E. Hemler. 2005. Metabolic activation-related CD147-CD98 complex. *Mol. Cell. Proteomics* 4: 1061–1071.
36. Wilson, M. C., D. Meredith, and A. P. Halestrap. 2002. Fluorescence resonance energy transfer studies on the interaction between the lactate transporter MCT1 and CD147 provide information on the topology and stoichiometry of the complex in situ. *J. Biol. Chem.* 277: 3666–3672.
37. Kirk, P., M. C. Wilson, C. Heddle, M. H. Brown, A. N. Barclay, and A. P. Halestrap. 2000. CD147 is tightly associated with lactate transporters MCT1 and MCT4 and facilitates their cell surface expression. *EMBO J.* 19: 3896–3904.
38. Melchior, A., A. Denys, A. Deligny, J. Mazurier, and F. Allain. 2008. Cyclophilin B induces integrin-mediated cell adhesion by a mechanism involving CD98-dependent activation of protein kinase C-delta and p44/42 mitogen-activated protein kinases. *Exp. Cell Res.* 314: 616–628.
39. Brini, M. 2009. Plasma membrane Ca(2+)-ATPase: from a housekeeping function to a versatile signaling role. *Pflugers Arch.* 457: 657–664.
40. Long, T., J. Su, W. Tang, Z. Luo, S. Liu, Z. Liu, H. Zhou, M. Qi, W. Zeng, J. Zhang, and X. Chen. 2013. A novel interaction between calcium-modulating cyclophilin ligand and Basigin regulates calcium signaling and matrix metalloproteinase activities in human melanoma cells. *Cancer Lett.* 339: 93–101.
41. Guo, N., K. Zhang, M. Lv, J. Miao, Z. Chen, and P. Zhu. 2015. CD147 and CD98 complex-mediated homotypic aggregation attenuates the CypA-induced chemotactic effect on Jurkat T cells. *Mol. Immunol.* 63: 253–263.
42. Strehler, E. E., and D. A. Zacharias. 2001. Role of alternative splicing in generating isoform diversity among plasma membrane calcium pumps. *Physiol. Rev.* 81: 21–50.
43. Caride, A. J., A. G. Filoteo, A. R. Penheiter, K. Pászty, A. Enyedi, and J. T. Penniston. 2001. Delayed activation of the plasma membrane calcium pump by a sudden increase in Ca2+: fast pumps reside in fast cells. *Cell Calcium* 30: 49–57.
44. Wu, G., X. Xie, Z. H. Lu, and R. W. Ledeen. 2009. Sodium-calcium exchanger complexed with GM1 ganglioside in nuclear membrane transfers calcium from nucleoplasm to endoplasmic reticulum. *Proc. Natl. Acad. Sci. USA* 106: 10829–10834.
45. Bautista, D. M., M. Hoth, and R. S. Lewis. 2002. Enhancement of calcium signalling dynamics and stability by delayed modulation of the plasma-membrane calcium-ATPase in human T cells. *J. Physiol.* 541: 877–894.
46. Niggli, V., and E. Carafoli. 1981. Interaction of the purified Ca2+, Mg2+-ATPase from human erythrocytes with phospholipids and calmodulin. *Acta Biol. Med. Ger.* 40: 437–442.
47. Baggott, R. R., A. Alfranca, D. López-Maderuelo, T. M. Mohamed, A. Escolano, J. Oller, B. C. Ornes, S. Kurusamy, F. B. Rowther, J. E. Brown, et al. 2014. Plasma membrane calcium ATPase isoform 4 inhibits vascular endothelial growth factor-mediated angiogenesis through interaction with calcineurin. *Arterioscler. Thromb. Vasc. Biol.* 34: 2310–2320.
48. Zhu, P., J. Ding, J. Zhou, W. J. Dong, C. M. Fan, and Z. N. Chen. 2005. Expression of CD147 on monocytes/macrophages in rheumatoid arthritis: its potential role in monocyte accumulation and matrix metalloproteinase production. *Arthritis Res. Ther.* 7: R1023–R1033.
49. Chen, X., J. Lin, T. Kanekura, J. Su, W. Lin, H. Xie, Y. Wu, J. Li, M. Chen, and J. Chang. 2006. A small interfering CD147-targeting RNA inhibited the proliferation, invasiveness, and metastatic activity of malignant melanoma. *Cancer Res.* 66: 11323–11330.
50. Curtin, K. D., R. J. Wyman, and I. A. Meinertzhagen. 2007. Basigin/EMMPRIN/CD147 mediates neuron-glia interactions in the optic lamina of Drosophila. *Glia* 55: 1542–1553.